

## A Simulation of Thermohaline Effects of a Great Salinity Anomaly

SIRPA HÄKKINEN

*NASA/Goddard Space Flight Center, Greenbelt, Maryland*

(Manuscript received 18 August 1997, in final form 10 June 1998)

### ABSTRACT

Model simulations of an idealistic “Great Salinity Anomaly” (GSA) demonstrate that variability in the sea ice export from the Arctic when concentrated to short pulses can have a large influence on the meridional heat transport and can lead to an altered overturning state. One single freshwater disturbance resulting from excess ice export, as in 1968, can disrupt the deep mixing process. The critical condition for a large oceanic response is defined by the intensity, duration, and timing of the ice pulse, in particular, as it exits through the Denmark Strait. A recovery from this event takes several years for advection and diffusion to remove the salinity anomaly. Concurrently, the influence of the GSA propagates to the subtropics via the boundary currents and baroclinic adjustment. As a result of this adjustment, there are large (up to 20%) changes in the strength of the overturning cell and in the meridional heat transport in the subtropics and subpolar areas. Simulations show a temperature–salinity shift toward colder and fresher subpolar deep waters after the GSA, which is also found in hydrographic data.

### 1. Background

In the present climate regime the renewal of the deep water masses in the northern North Atlantic depends on a conversion of light water to bottom water mainly through heat loss while the freshwater flux opposes the process. The “recent” occurrence of the Great Salinity Anomaly (GSA), in the end of the 1960s, early 1970s in the northern North Atlantic (Dickson et al. 1988) resulted in very fresh surface conditions occupying the subpolar gyre for several years. Occurrence of GSA shows that the balance between the thermal and haline contribution to the surface buoyancy flux could be rather delicate. Dickson et al. estimated the excess freshwater associated with this event to be about 2300 km<sup>3</sup>. Compared to the last glacial period meltwater pulse, this was a very modest disturbance. However, as a decadal-scale climate event it is rather significant, as the observational studies by Levitus (1989) have documented its widespread influence in the hydrography of the North Atlantic by comparing pentads of 1955–59 and 1970–74. Also the GSA caused a cessation of convection in the Labrador Sea as recorded at Weather Station Bravo by Lazier (1980). Greatbatch et al. (1991) and Ezer et al. (1995) have investigated the dynamic influence of the changes in hydrography between the above-mentioned pentads before and after the GSA using diagnostic mod-

els. Their studies imply that there was a 30% decrease in the strength of the Gulf Stream system. Associated with decreased western boundary currents, Greatbatch and Xu (1993) estimated that the meridional heat transport change from the 1950s to 1970s was about 0.2 PW at subtropical and subpolar latitudes. The changes in the subtropical circulation are associated with a decrease in north–south steric height, which has been also corroborated by coastal tide gauge data (Ezer et al. 1995).

While there may have existed large changes in the thermal component of the surface buoyancy loss contributing to the GSA, this study concentrates on exploring changes in the haline component of the surface buoyancy flux. The high latitudes are characterized by net precipitation; however, sea ice melt gives an equally important contribution to the surface freshwater flux, and depending on the location it can be even the prime contributor to the total surface buoyancy flux. The sea ice export from the Arctic is about 2000–2800 km<sup>3</sup> [the former estimate is from Vinje et al. (1996, manuscript submitted to *J. Geophys. Res.*); the latter estimate is from Aagaard and Carmack (1989)]. This amount of ice melt is approximately as large as the annual net precipitation – evaporation ( $P - E$ ) in the Greenland–Iceland–Norwegian (GIN) Seas and in the subpolar gyre together [the estimate is based on National Meteorological Center (NMC, now known as the National Centers for Environmental Prediction) data (Rasmusson and Mo (1996))]. As for the variability of ice export, observational data is still limited but suggests the same conclusion as numerical modeling that the variability in the

---

*Corresponding author address:* Dr. Sirpa Häkkinen, NASA/Goddard Space Flight Center, MC 971, Greenbelt, MD 20771.  
E-mail: hakkinen@gsfc.nasa.gov

sea ice transport from the Arctic can be as large as the mean. Furthermore, the modeling simulations (Häkkinen 1993, 1995) suggest that the excess freshwater associated with the GSA could be explained by excess sea ice transported from the Arctic based on a hindcast simulation.

The thermohaline system response to hydrological forcing changes have been explored by several authors in the past. Considering the oceanic response to a large freshwater flux disturbance, Manabe and Stouffer (1995) used a pulse of  $300\,000\text{ km}^3$  during a 10-yr period, such as may have occurred as a result of glacial melt before the Younger Dryas. Their coupled model response shows an initial (near) collapse of the thermohaline circulation then a rapid recovery and yet another collapse before slow recovery with modest oscillations during a couple hundred years. Nevertheless, while the ocean was advecting and diffusing the initial anomaly, a recovery occurred approaching a similar strength of the control case. On the other end of the scale of more modest disturbances, Rahmstorf (1995b) using small incremental freshwater flux increases, shows the resulting thermohaline system hysteresis and multiple equilibria, which depend on the initial state. The rapid decay of the thermohaline circulation appears to start with an annual freshwater flux anomaly (referenced to the present climate) of  $0.06\text{ Sv}$  [corresponds to freshwater excess of  $2000\text{ km}^3$  annually;  $\text{Sv} \equiv 10^6\text{ m}^3\text{ s}^{-1}$ ] when initialized from the oceanic equilibrium corresponding to the present climate (or a similar state, as several equilibrium states exist). An alternative approach to estimate this critical freshwater excess is from surface buoyancy flux information, but observational ice melt values are lacking: using the quasi-equilibrium run of Mauritzen and Häkkinen (1997, hereafter MH), which includes model estimate of the ice melt, the annual freshwater excess that is needed to remove all buoyancy loss between  $45^\circ\text{N}$  and  $80^\circ\text{N}$  is about  $3500\text{ km}^3$ . This is rather close to the value of the freshwater flux anomaly of Rahmstorf (1995b) of  $0.1\text{ Sv}$  where the thermohaline circulation collapses in his model. This study will show that the effect of a GSA-like freshwater disturbance on the thermohaline circulation is to shift the deep convection sites and overturning rate compared to the undisturbed run. This shift in the thermohaline system appears in the model as the freshening of the deep waters. Observations also show that after the passage of GSA, the deep waters freshened in the 1970s and 1980s in the Labrador Sea (Swift 1984). The investigation focuses on the time evolution of some of the integral quantities of the system like the overturning rate, meridional heat transport, horizontal transport, freshwater budget, and deep water temperature–salinity ( $T$ – $S$ ) properties.

Although the observational evidence supports that the GSA was a major climatic event, a modeling study by Power et al. (1994) suggests that a freshwater excess of one or two GSA, distributed evenly over 5 yr (north of

the sills, into the Greenland Sea), causes hardly any changes in the overturning cell. Their results suggest that it takes seven to eight times the GSA freshwater anomaly to be added to the system before a collapse of the thermohaline cell occurs. On the other hand, MH showed that a persistent difference of  $800\text{ km}^3$  in ice export to the subpolar gyre for 5–10 yr produces a considerably different oceanic response with 10%–20% differences in meridional heat transport and up to  $2.5\text{ Sv}$  amplitude in the meridional overturning cell (MOC). If one would assume linear variability about the equilibrium oceanic state, the maximum MOC change using Power et al.'s approach (from one GSA over 5 yr in the GIN Sea) would result in at most  $1.3\text{ Sv}$  change in MOC. Furthermore, if only 50% of that freshwater pulse exits Denmark Strait (since a large recirculation exists in the GIN Seas), the MOC change would be only about  $0.5\text{ Sv}$ . This would favor the conclusions of Power et al. that no major effects on MOC were exerted by a freshwater anomaly of one GSA.

To understand the disparity between the observational evidence of a significant climate event and the results of Power et al., this study considers whether a seasonally phaselocked freshwater anomaly can produce as large changes as observed in the northern North Atlantic. Especially we consider a pulse of freshwater that is introduced to the Labrador Sea via sea ice export during fall and winter seasons. The observed cessation of the Labrador Sea Water (LSW) production possibly due to the thermal component of the buoyancy flux is not addressed in this study, only the freshwater contribution to the oceanic variability is investigated. However, it is known that at the low phase of the North Atlantic oscillation (NAO), which occurred in the end of 1960s (Hurrell 1995) coinciding with GSA, the subpolar gyre winds are weak. The weak winds in turn are associated with a decreased oceanic heat loss, which would contribute further to the decreased overturning. In fact, the low phase of NAO is conducive of large ice export from the Arctic as a strong high pressure center is located over Greenland enhancing the anticyclonic circulation of the Arctic and subsequently ice outflow. Thus, during GSA both the surface heat loss due to the weak winds and ice conditions would indeed have been amplifying each other's influence on the thermohaline system. A review of observations on hydrographic and convective conditions in the polar and subpolar North Atlantic and their relation to NAO is given in Dickson et al. (1996).

The coupled ice–ocean model used in this study has been previously presented in studies by Mellor and Kantha (1989) and Häkkinen and Mellor (1992) with a more detailed model description. The quasi-equilibrium runs, to which the effects of an idealistic GSA are compared, are presented in MH. The ice and ocean models and their initialization are briefly summarized in section 2. The model results are presented in section 3 from two GSA experiments in which the model initialization originates from the two above-mentioned quasi-equilibrium

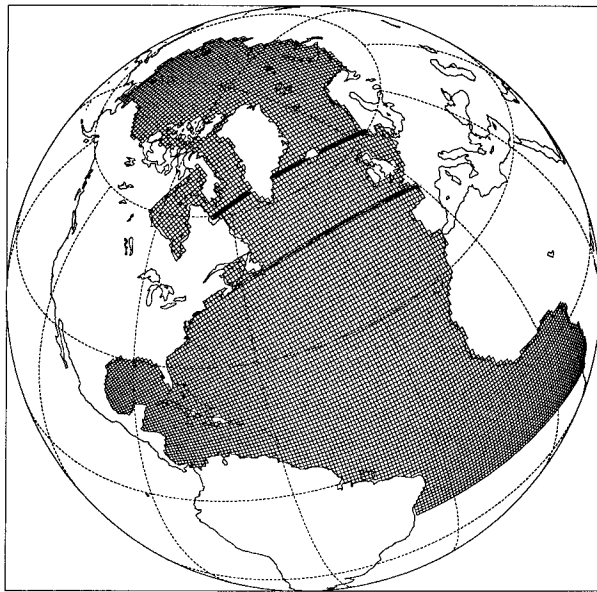


FIG. 1. Model grid. The thick lines (at about 45°N and 65°N) are used to define the subpolar gyre.

runs, one with a weak overturning and one with a rigorous overturning. In the previous case the annual Arctic ice export is 2800 km<sup>3</sup> (experiment 1 of MH). In the second case the annual export is about 2000 km<sup>3</sup> (experiment 2 of MH). All experiments use atmospheric monthly climatology except on the first year of the GSA simulation where 1968 wind stress was invoked in the Arctic and GIN Seas.

## 2. The coupled model

### a. Model description and model grid

The ocean model is hydrostatic, Boussinesq, and uses the sigma-coordinate system as described in Blumberg and Mellor (1987) with a modified scalar advection scheme to avoid overshooting at sharp fronts (MH). The 2.5-level turbulence closure scheme of Mellor and Yamada (1982) is used to determine the vertical mixing coefficients for momentum and scalar variables. The dynamic–thermodynamic ice model is coupled to the ocean model via interfacial stresses and via salinity and heat fluxes through the ice–water interface. The ice model uses a generalized viscous rheology as discussed in Häkkinen and Mellor (1992).

The coupled ice–ocean model extends from the Bering Strait to 15°S with resolution of 0.9° lat, 0.7° long (in a rotated coordinate system with an equator at 30°W and the pole at 0°, 120°W) (Fig. 1). There are a total of 20 sigma-levels in the vertical with higher resolution near the surface. To minimize the inaccuracies in the computation of the pressure gradient, the topography (derived from the TerrainBase Global DTM database with 5' × 5' resolution) is smoothed heavily.

### b. Initialization and forcing of the coupled model

The initialization of the GSA simulations are taken from the end of the 10th simulation year of two quasi-equilibrium runs presented in MH as experiments 1 and 2; the corresponding GSA runs are called GSA1 and GSA2. By the 10th year the midlatitude Rossby adjustment (first mode) has taken place while the deep ocean evolves slowly. The system is assumed to be linear enough for anomalies to behave as anomalies for a system at equilibrium (i.e., to assume that any nonlinear effects of the further adjustment of the control and perturbation runs are negligible). The quasi-equilibrium runs (experiments 1 and 2) were initialized with the annual average hydrographic climatology of Levitus (1982). The volume transports at oceanic lateral boundaries were specified to be 0.8 Sv (Aagaard and Carmack 1989) at the Bering Strait, and 0.8 Sv out at 15°S. At the southern boundary the baroclinic velocity field is determined from geostrophy. At the southernmost grid row the temperature and salinity are computed using upstream-advection scheme and Levitus values at inflow points. A further relaxation to Levitus values is applied for four grid rows from the boundary. Restoring of temperature ( $T$ ) and salinity ( $S$ ) is used at the Mediterranean outflow point.

The model is forced with atmospheric climatological data except for the first year of the GSA runs. The momentum exchange between the atmosphere and ice-ocean are specified from the Trenberth et al. (1989) monthly European Centre for Medium-Range Weather Forecasts (ECMWF) wind stress climatology over open ocean and a geostrophic wind stress [derived from National Center for Atmospheric Research (NCAR) 5 × 5 surface pressure climatology) over sea ice with an exchange coefficient of 1.3E−3]. For the first GSA simulation year, the wind stress is modified north of Iceland by invoking the geostrophic wind stress of 1968. Both in the climatological case and the 1968 wind stress case, blending and binomial smoothing was used at the boundary of the different wind stress products to minimize formation of a spurious wind stress curl. The experiments show that 1968 was very favorable in creating a large ice export pulse. Additionally the model uses modulation of the ice shear viscosity to enhance the event because the ice cover has memory for 5–10 yr (a renewal time of the ice cover based on the timescale defined by Arctic ice mass divided by the annual Fram Strait ice export), so the 1968 event in reality was a final result of special atmospheric conditions prevailing for several years over the Arctic.

For the heat exchange, the bulk formulation is adopted for the sensible and latent heat, which are derived with exchange coefficient of 1.3E−3 from the ECMWF monthly climatologies of wind, temperature, and humidity and model-generated surface temperature and derived specific humidity with 98% saturation. Shortwave and downward longwave radiation require cloudiness

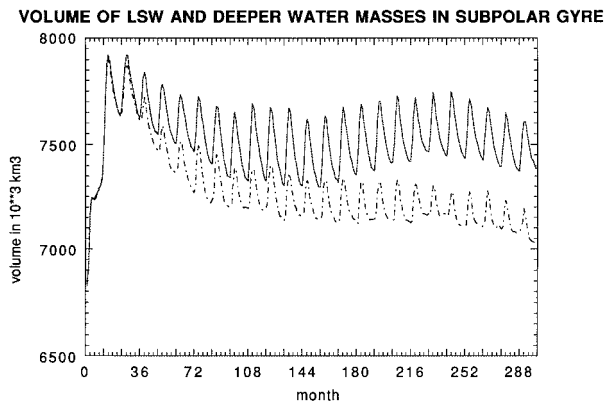


FIG. 2. Volume of LSW and deeper water masses (density  $\geq 27.7 \sigma_0$  units) in subpolar gyre (defined in Fig. 1) for experiments 1 (dashed line) and 2 (solid line) for 25 simulation years. GSA simulations start after month 120.

information, which is given by International Satellite Cloud Climatology Project measurements. The surface boundary condition for  $S$  is a virtual salt flux where the  $P - E$  field is obtained from NMC operational analysis (Rasmusson and Mo 1996) averaged for 5 yr. When the river runoff [from Pocklington (1987) and Russell and Miller (1990)] with an annual total of  $18\,000 \text{ km}^3$  is included, modifications were added to the  $P - E$  field at  $8^\circ\text{--}12^\circ\text{N}$  to conserve salt in the basin. The above choices for the surface boundary condition for  $T$  and  $S$  are in effect the so-called mixed boundary conditions. The above computation of all heat flux components is necessary because of the sea ice model, which requires solving the snow-ice surface temperature from the surface heat balance. If there is a heat gain at the surface, the heat is used to melt snow and ice, otherwise the flux has to balance the heat conduction through ice. Any imbalance in the heat flux at the ice-ocean interface is used either to melt ice or for freezing.

### 3. Results

The two idealistic GSA runs discussed here are called GSA1 and GSA2, which are initialized from the end of the 10th simulation year of the quasi-equilibrium runs experiments 1 and 2, respectively. The two runs, experiments 1 and 2, use exactly the same surface atmospheric forcing and the same river runoff and lateral boundary conditions. The only difference is that the sea ice in experiment 2 (and GSA2) is twice as viscous as in experiment 1 (and GSA1), which leads to two major differences: 1) experiment 1 has a larger Arctic ice export (by  $800 \text{ km}^3$ ) than experiment 2, and 2) most of this change in ice export influences the subpolar gyre, making convection more extensive and vigorous in experiment 2 than in experiment 1 and subsequently experiment 2 has an overturning cell that is 2–3 Sv stronger than in experiment 1. This change is caused by the smaller freshwater flux (from ice melt) of experiment 2

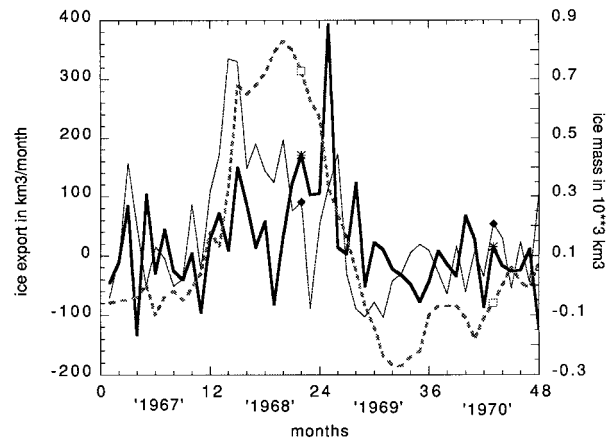


FIG. 3. Ice exports from Häkkinen (1993) at Fram and Denmark Straits superimposed with the GIN Seas ice mass anomaly. Anomalies are referenced to the 1955–85 run of Häkkinen (1993, 1995). Thin solid line is Fram Strait ice export, thick solid line is Denmark Strait ice export, and dashed line is the GIN Seas ice mass anomaly.

in the subpolar gyre. There is a significant difference in response between these two runs to the added freshwater in the subpolar gyre for which the ultimate cause is the LSW formation or lack of it in the quasi-equilibrium run: In experiment 1 there is a gradual decrease in the LSW (density  $\geq 27.7 \sigma_0$  units) and deeper water mass volume (and in the seasonal amplitude) with time while in experiment 2 that same water mass volume is quite stable for the duration of the simulation (Fig. 2).

On the first year of the GSA runs the 1968 wind stress is applied north of  $60^\circ\text{N}$ , otherwise the ECMWF wind stress climatology is used everywhere else. All other surface forcing is climatological monthly data. For the second year and all following years the wind stress forcing returns back to climatology. It turns out that the response in GSA2 is much larger than in GSA1 and the return to near-normal (at least in some aspects) conditions takes much longer time, thus the GSA2 run is extended to 15 yr while the GSA1 run is a 10-yr run.

#### a. Sea ice

To provide some background to the concept of a short and large pulse of ice entering a key water mass formation area such as the Labrador Sea, the ice export in the model results of Häkkinen (1993, H1993 from here on) are revisited here to gain new insights. H1993 used monthly climatology for all other atmospheric forcing components except for (geostrophic) daily wind stress and wind speed derived from the NCAR  $5 \times 5$  surface pressure dataset. Based on this simulation, the excess ice export at Fram Strait (during 1968),  $1700 \text{ km}^3$  above the simulation average of  $2000 \text{ km}^3$ , was distributed rather evenly throughout the year. However, a large portion of this imported sea ice accumulated in the Greenland Sea and did not exit through the Denmark Strait until late fall 1968 and early the following winter (Fig.

3). Altogether, the excess ice export through the Denmark Strait was about 900 km<sup>3</sup> during the 6-month period, October 1968–March 1969. Timing of this freshwater pulse has a strong effect on convection downstream because in late fall–early winter, the new deep waters are formed through densification driven by thermal fluxes with freshwater fluxes opposing the process. However, besides timing, the intensity of the pulse, 900 km<sup>3</sup> of freshwater in a few months, is equally important. Also noteworthy is that the Fram Strait ice export was much lower than average for several years before the 1968 event (H1993), which would make the 1968 export event nearly three times the preceding annual exports.

With this guidance from the limited-area model, the simulated ice export volume can be modulated in an Arctic–North Atlantic model by changing the ice shear viscosity. Thus we can arrive at an idealized simulation of the GSA and its effects downstream without requiring a full-blown long-term simulation with interannually varying forcing. The two simulations, GSA1 and GSA2, have an anomalous ice mass accumulation in the Greenland Sea (Fig. 4a) shown against the limited-area model ice mass anomaly (shifted in y axis). In H1993 the total ice export from the Arctic was 1700 km<sup>3</sup> above the equilibrium. In GSA1 and GSA2, the total ice export from the Arctic is 3355 and 3207 km<sup>3</sup> above the equilibrium (of 2664 and 1907 km<sup>3</sup>, respectively) for the first year and is close to zero for the following years. These exports are much larger than in the limited-area model, but most of this ice export does not exit to the subpolar gyre, as the excess ice export to the Labrador Sea is 1170 and 1240 km<sup>3</sup> in GSA1 and GSA2, respectively during the 6-month period covering October–December of the first year and January–March of the second year. These ice melt anomalies constitute about 50% of the climatological freshwater ( $P - E$ ) flux to the subpolar gyre (estimated from Rasmusson and Mo 1996). It will be seen that it is mainly the ice export part entering the subpolar gyre that influences the thermohaline circulation. Figures 4b,c show these exports with the H1993 ice exports. The GSA runs capture well the variability in ice exports as simulated by the limited-area model with more realistic wind forcing.

*b. Horizontal circulation changes*

The excess ice mass from the Greenland Sea enters the Labrador Sea during the period of deep mixing in wintertime, thus disrupting the convective processes that are directly responsible for the formation of the LSW. LSW is a part of the Deep Western Boundary Current (DWBC), so an interruption in LSW formation will influence the DWBC by reducing its transport. The adjustment to the new buoyancy forcing and changes in the DWBC are propagated farther downstream through Rossby topographic waves (fast adjustment time, propagation to the equatorial region occurs within a couple of months) (Hallberg and Rhines 1996) and by advective

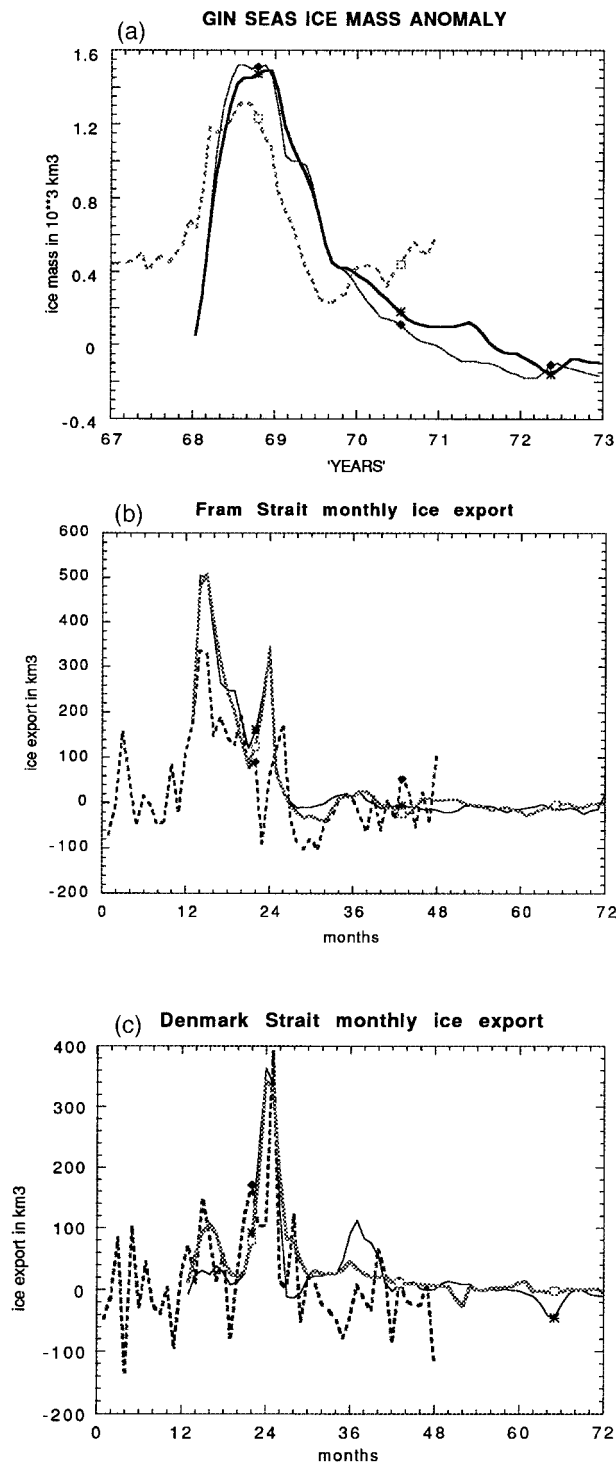


FIG. 4. (a) Ice mass anomaly in the GSA1 and GSA2 experiments together with Häkkinen (1993) anomaly (shifted in y axis). (b) GSA1/2 ice export anomalies at Fram Strait and at (c) Denmark Strait. A thin solid line refers to GSA1, a thick solid line refers to GSA2, and a dashed line refers to H1993.

tion of the modified water mass in DWBC (Kawase 1987) and on longer timescales ( $\sim 5\text{--}6$  yr) by arrival of Rossby waves at the western boundary.

The studies of Greatbatch et al. (1991) and Ezer et al. (1995) suggest that there could be a 30% weakening in the Gulf Stream strength during the GSA. Greatbatch et al. (1991) show that most of this influence on the barotropic transport comes from the Joint Effect of Baroclinicity and Relief (JEBAR). They conclude that most of the JEBAR effect arises from the changes in baroclinic structure in the upper 1500 m, especially that the wind stress changes were minimal during the pentads studied. In this study, the differences in the horizontal transports in the case of experiment 1–GSA1 are negligible (only a couple of Sverdrups; not shown), but in the case of GSA2 the maximum changes at the Gulf Stream region off Cape Hatteras reach over 10 Sv (i.e., weaker transport in GSA2) at year 6 (Fig. 5b), where the difference is referenced to the parallel run experiment 2 (Fig. 5a). The net transport across the section in the Gulf Stream marked in Fig. 5 is about 40 Sv, thus the change of 10 Sv corresponds to weakening of the Gulf Stream system by 20%–30% and these decreased transports prevail for several years. The area of influence is limited to the boundary of the subtropical and northern recirculation gyres and to the subpolar gyre. The appearance of the simulated transport changes over the Gulf Stream and North Atlantic Current is somewhat different from the diagnostic studies. However, the diagnostic studies rather correctly describe the strong Gulf Stream recirculation (the southern gyre), which is missing in this model and the weakening of the Gulf Stream is actually concentrated to this recirculation area in these diagnostic studies.

### c. Changes in the meridional overturning cell and heat transport

Since there are changes in the DWBC, changes in the meridional overturning can be expected. There is a difference whether meridional overturning cell (MOC) is computed at  $z$  levels or density surfaces, especially in the subpolar gyre where water masses of different density are moving in opposite directions at the same depth level and cancel each other in zonal averaging. MOC of experiment 2 on  $z$  levels at year 15 is shown in Fig. 6a. MOC in experiment 1 is very similar in appearance but the midlatitude maximum is weaker by 2–3 Sv. While the  $z$ -level rendition of the MOC shows nearly no overflow (Fig. 6a) and the cell does not extend continuously to  $60^\circ\text{N}$ , in density space, MOC with flow referenced to  $\sigma_{-1} = 32.3$  (about  $\sigma_{-0} = 27.7$ , the thermocline water) is about 25 (22) Sv at  $45^\circ\text{--}60^\circ\text{N}$  in experiment 2 (1). The Nordic sills overflow referenced to  $\sigma_{-1} = 32.42$  is about 6.5 Sv in both experiments 1 and 2. The model weakness is that most of the deep water overflow occurs between Iceland and Scotland with a very small amount through the Denmark

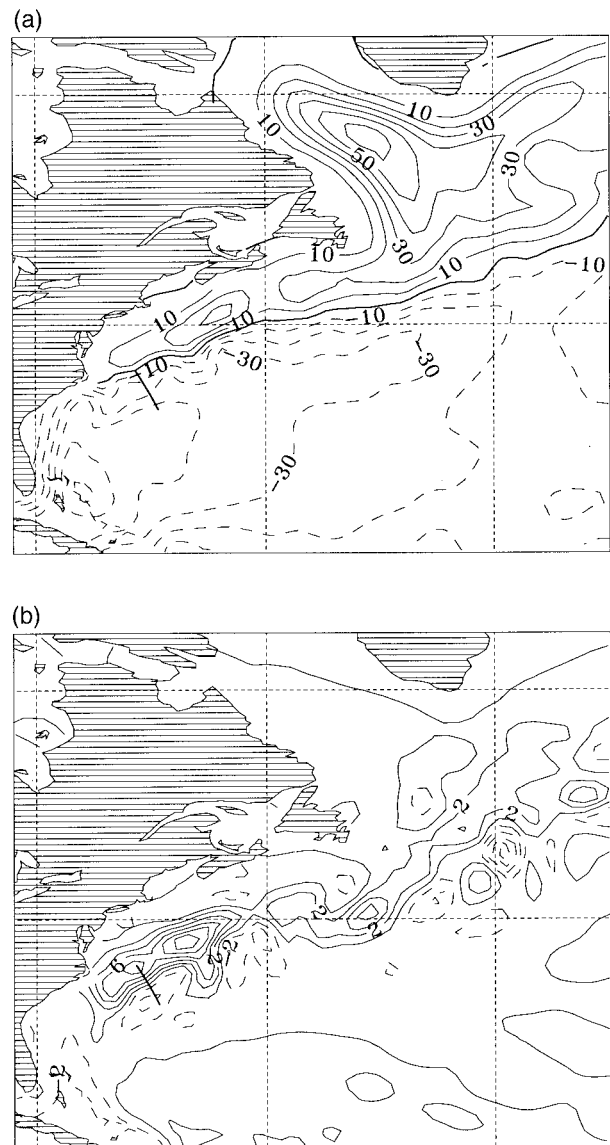


FIG. 5. (a) Horizontal streamfunction at year 6 in experiment 2 and (b) anomalous transports in the GSA2 run (i.e., experiment 2–GSA2), both are annual averages. Contour interval is 10 Sv in (a), and 2 Sv in (b).

Strait. More discussion of MOC in this model and its sensitivity to changes in surface forcing is provided in Mauritzen and Häkkinen (1998).

The simulated MOC anomalies due to the GSA event are the most prominent during years with 5–7 Sv at midlatitudes. MOC anomaly in GSA1 is at most 1 Sv at year 5 (not shown), but in GSA2 the response is much larger, up to 2.5 Sv (shown in Figs. 6b–d for years 5–7 as annual averages). The monthly midlatitude maxima reach 3–4 Sv during the course of those years. The MOC variability referenced to a density surface of  $\sigma_{-1} = 32.3$  at  $25^\circ\text{N}$  and  $45^\circ\text{N}$  are shown in Figs. 6e,f; values are smoothed by a binomial filter. At  $25^\circ\text{N}$ , GSA1 has

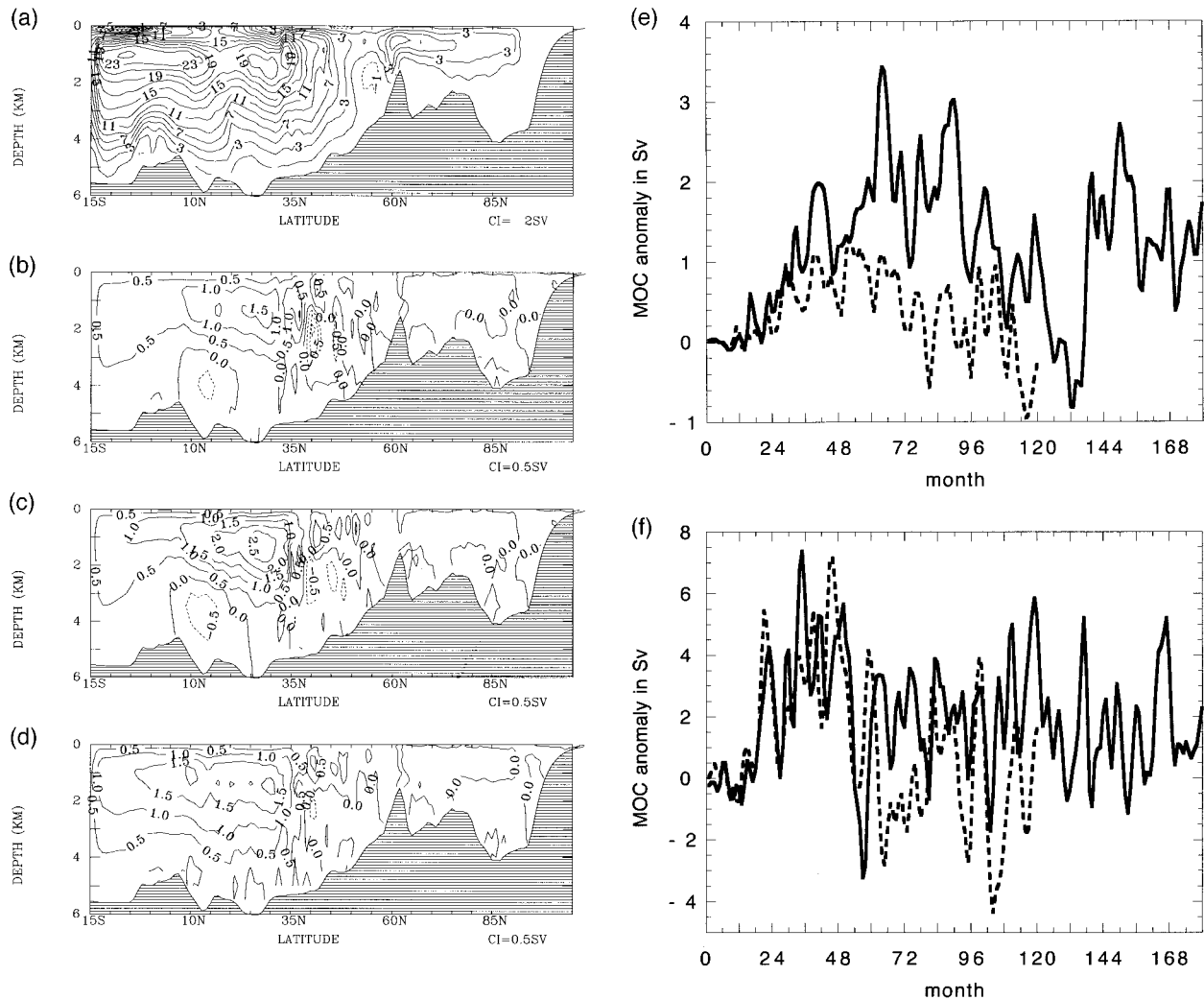


FIG. 6. (a) Meridional overturning cell at year 15 in experiment 2, contour interval is 2 Sv. (b)–(d) MOC anomalies (experiment 2–GSA2) at years 5–7 as annual averages with contour interval of 0.5 Sv. Time evolution of the anomalous MOC with flow referenced to density at  $\sigma_1 = 32.3$  for GSA1 (dashed) and GSA2 (solid) (in Sv) (e) at 25°N and (f) at 45°N (a binomial filter used once to smooth the data).

a decrease of 1.0–1.5 Sv at maximum (Fig. 6e), which lasts only a couple of months during year 5. The largest deviations in GSA2 are about 3–4 Sv, which dominate the summers of simulation years 5–7. This magnitude change is about 20% of the standard simulation overturning cell. At 45°N, closer to the source of the disturbance, the deviations are much larger (Fig. 6f), reaching over 6 Sv in both runs. The return of convection is marked by negative anomalies at year 4, which linger much longer in GSA1. The reasons for the return of convective conditions are discussed in the section 3d. The anomalies in the  $z$  level and density level MOC are similar in both of the cases for the latitude band 15°N–30°N; however, farther north the  $z$ -level MOC anomaly does not register the considerable changes in the LSW volume transport. The midlatitude response can be interpreted to reflect decreased upwelling of deep waters (mainly LSW) to the thermocline, which diminishes due

to the decreased production of LSW. North of the latitude band, the simultaneous Gulf Stream–North Atlantic Current weakening compensates the changes in DWBC zonally. South of 15°N the MOC changes in GSA2 are smaller but do extend to the southern boundary, which will change the whole basin quantities such as the salt content (section 3f). In GSA1 the response is limited to the subpolar gyre and midlatitudes. The influence of the GSA event on the NADW overflow was insignificant in both of the simulations: in the control runs the overflow is 6.5–6.6 Sv, while at the end of the GSA1 and GSA2 runs there is a decrease less than 0.2 and 0.5 Sv, respectively. These amounts constitute less than 7% change compared to the control runs.

It is apparent from Fig. 6c that MOC of GSA2 did not return to the strength of the parallel run but is about 0.5–1.0 Sv weaker. Lenderink and Haarsma (1994) and Rahmstorf (1995a,b) have discussed the sensitivity of

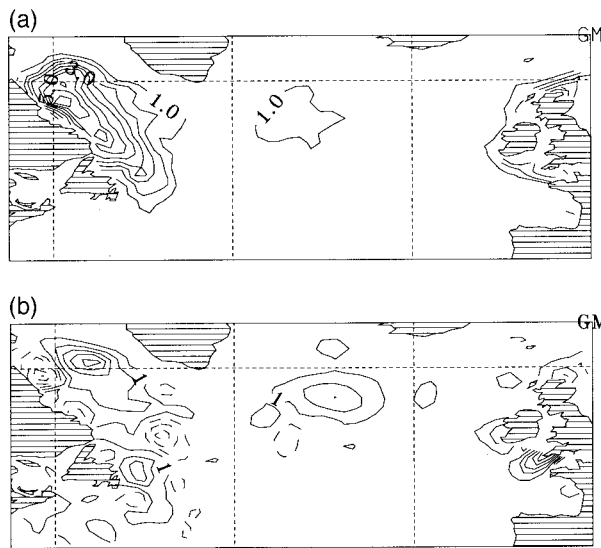


FIG. 7. (a) TKE ( $\text{cm}^2/\text{s}^2$ ) for experiment 2. (b) TKE difference ( $10^{-1} \text{ cm}^2/\text{s}^2$ ) experiment 2–GSA2. Both in March of year 10 of the GSA2 simulation.

the overturning to the location of the deep convection, in other words, mass compensation depends on the site where sinking occurs. The subpolar gyre can be divided into several categories: convective, nonconvective, periodic, and areas where convection can be easily started or turned off. To assess this hypothesis of a shift in convection sites as the reason for the difference in overturning rate between experiment 2 and GSA2, we plot the turbulence kinetic energy (TKE) for the undisturbed run and the difference experiment 2–GSA2 (vertical average) for the month of March when winter convection is the most intense, (Figs. 7a,b for year 10). Since the wind stress is the same in experiment 2 and GSA2, any resulting differences in the vertically integrated TKE reflect how deep turbulent mixing due to wind stirring and convection can reach as a result from changes in stratification. Figure 7a shows the predominant deep mixing areas in the main North Atlantic basin to be at the east coast of Newfoundland, central Irminger Sea, and west of the British Isles. Figure 7b shows that there are shifts in the convection sites, especially in the Labrador Sea, that persist over several years.

Along with the changes in the overturning cell, one expects changes in the meridional heat transport (Fig. 8). The maximum heat transport decreases as much as 0.2 PW and most prominently during summer months. For comparison the meridional heat transport of experiment 2 is 1.3 PW at  $25^\circ\text{N}$ . The seasonality of the heat transport changes is associated with the timing of the LSW water (now greatly reduced) leaving the subpolar gyre. Typically the changes are 10%–20% of the monthly mean depending on the location. The largest changes in the subtropical gyre area take place on the sixth simulation year when the overturning is at the minimum.

#### d. SST and SSS anomalies

The surface expression of the aftermath of the idealized GSA event is shown in Fig. 9 for GSA2 (but GSA1 is very similar but slightly weaker) as winter (Jan–April) anomalies for sea surface temperature (SST) and sea surface salinity (SSS) for years 2–5. The fields are deviations from the corresponding equilibrium run (GSA–experiment). During the second year there is a large positive salinity anomaly around the periphery of the Arctic where most of the sea ice is produced and transported via the Transpolar Drift Stream to the GIN Sea. Freshening and cooling downstream is limited to the Labrador Sea from where it will slowly disperse with advection during the following years. At year 5 there are still remnants of the event in the northern sections of the Labrador Sea while the southern section is recovering and even shows a weak positive SST anomaly indicative of either intrusion of Atlantic water or deep convection.

To show another perspective for the SST and SSS anomalies the monthly variability of the area average anomalies is plotted for the Arctic, GIN Seas, and Labrador Gyre (west of  $30^\circ\text{W}$ ), in Figs. 10a–c (as a difference GSA–experiment). The Arctic (Fig. 10a) shows that during the first summer (with an extensive ice export) there is a considerable warming of the upper ocean due to the decreased ice cover. This anomaly decays substantially by the second summer after which the dissipation of the summer SST anomalies is much weaker and takes nearly 10 yr to return to normal temperatures. The positive SSS anomaly, a more saline upper layer than during normal conditions, results from increased ice production in leads created by the export pulse. It also shows large seasonal fluctuations but recovery toward normal conditions is slow after year 6. The full recovery of the Arctic surface salinity may take decades to be completed in both GSA simulations. In the GIN Seas (Fig. 10b) the SST anomaly is opposite to the Arctic one, warm surface layers are typical of normal conditions, and cool surface reflects freshwater or ice capping of the water column. During the first 2 yr the cold anomalies are pronounced but are reversed briefly due to enhanced convection (due to transport of salty upper-layer waters from the Arctic) before returning to more or less normal conditions within 10 yr. The SSS anomalies are quite parallel to the SST anomalies but show more clearly the removal of the freshwater capping by more saline waters after year 4. The more saline surface conditions derive from advection of saline Arctic surface waters into the area, and since the main Arctic stays more saline than normal for the length of the simulation in GSA2, the SSS in the GIN Seas is not returning to normal conditions either.

The area average SSS and SST anomalies in the Labrador Sea (Fig. 10c) show cool and fresh conditions to dominate for the first 5–6 yr in GSA1 and GSA2. The freshening signal is much stronger in summertime due

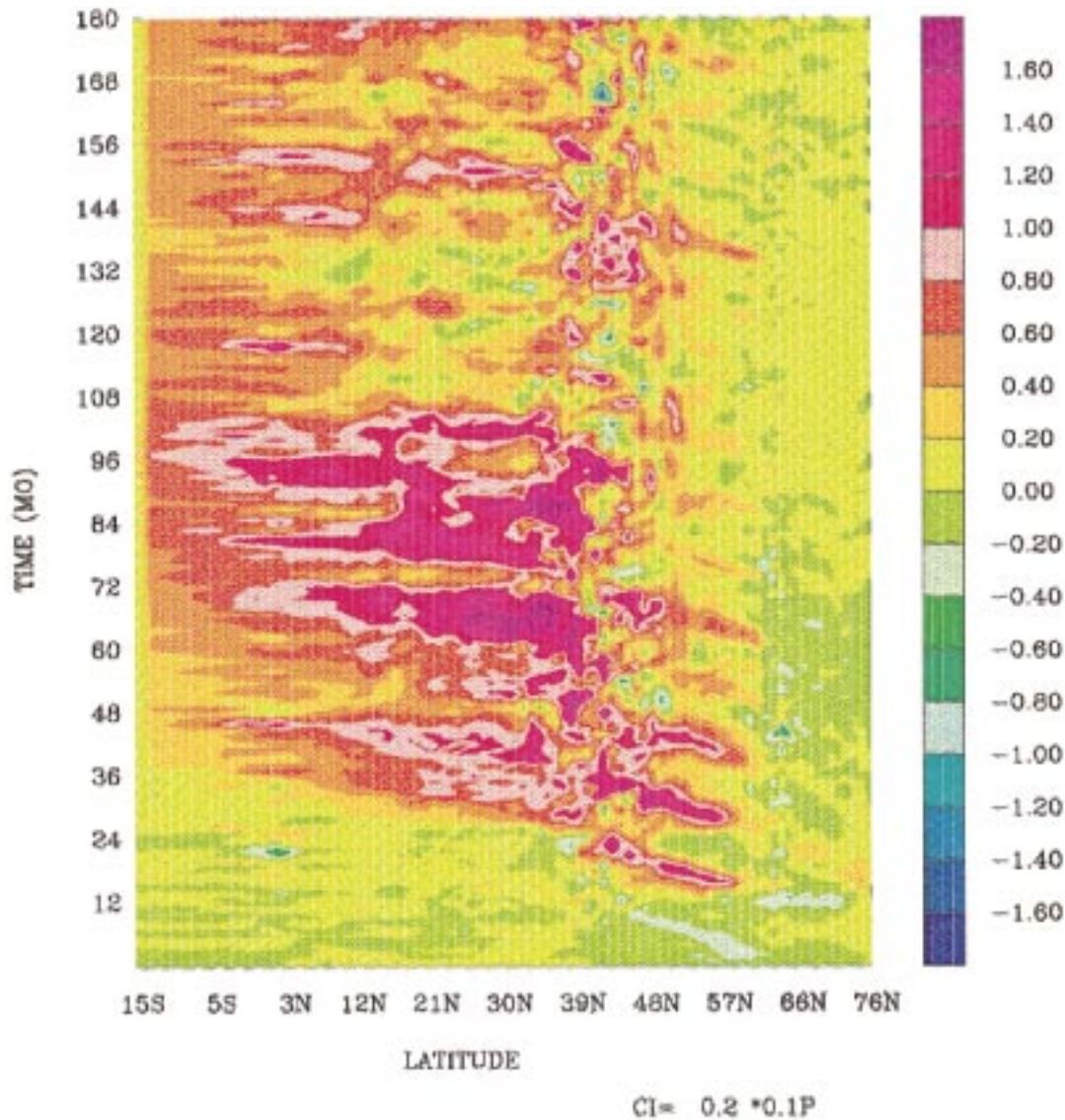


FIG. 8. Time evolution of the meridional heat transport anomaly for experiment 2–GSA2 in  $10^{14}W$ .

to the local rainfall–ice melt accumulation resulting from diminished mixing associated with stronger stratification. Cold SST is found only during winters, summers are actually warmer than normal because the fresh-water layer prevents mixing of heat downward. At year 4 in GSA2 and year 5 in GSA1 there is a lack of the seasonal anomaly maximum, which is a sign of a partial return of convective conditions in the Labrador Sea. The the anomalous surface conditions disappear during year 6 in GSA1 and during year 7 in GSA2 after saline surface waters of Arctic origin, which are somewhat modified in the GIN Seas, finally arrive at the area. Also local advection in the subpolar gyre of the fresh anomaly and its interaction with imported surface waters has influence, otherwise GSA1 and GSA2 would have a reversal at the same time. The increased convection in

GSA1 is clearly reflected in the increased surface salinity, which will approach normal conditions by year 10. In GSA2 the salinities return to near-normal conditions after year 6 but freshen afterward somewhat. Similarly the SST anomaly in GSA2 stays cooler at average than in the control run.

As the surface behavior suggests, the Labrador Gyre appears to operate normally in the GSA2 run after recovery but has shifted in TS space to fresher and colder water masses after year 7. Inspection of TS space of the water columns sampled from the subpolar gyre in March at year 10 and 15 (Figs. 11a,b) confirms this: While the densities stayed nearly the same there is a significant shift in TS space all the way to the bottom. Figure 11a shows TS properties for three points east of Newfoundland, in the area of LSW formation, thus the very narrow

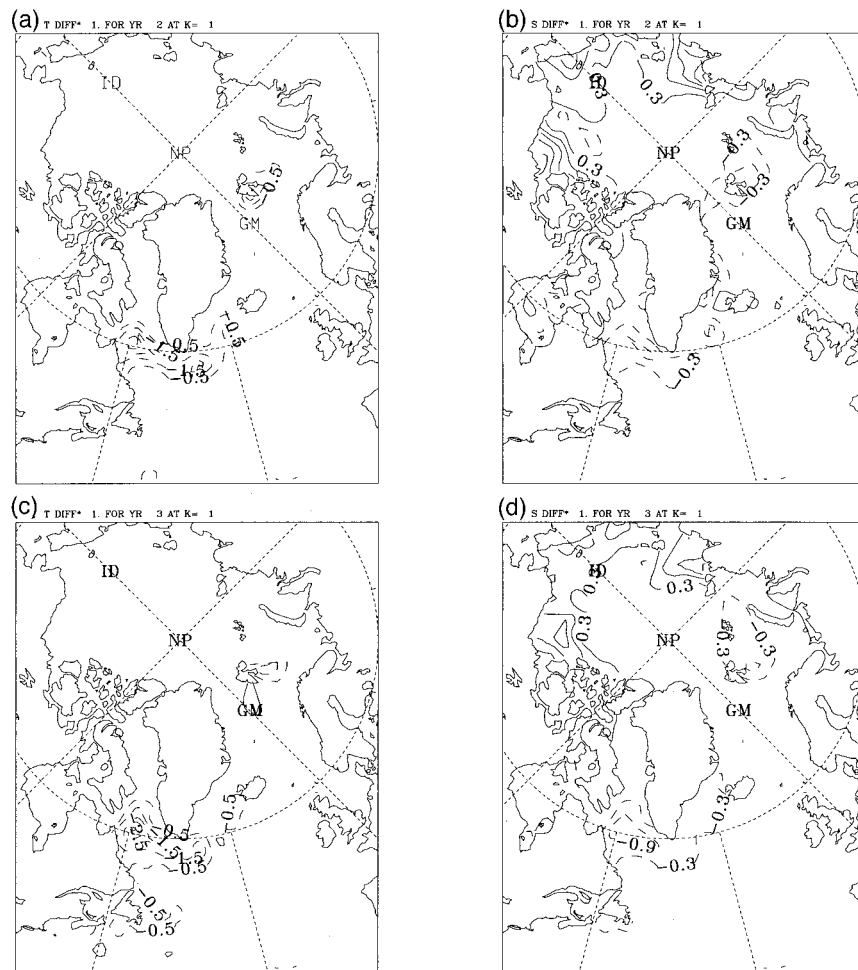


FIG. 9. Spatial distribution of the winter anomalies (GSA2-experiment 2) (Jan–Apr) for SST and SSS, contour intervals are  $1^{\circ}\text{C}$  and  $0.6$  ppt.

density range. Figure 11b shows two points selected from the central subpolar gyre farther east dominated by North Atlantic Current waters and where convection does not penetrate beyond 200–300 m. Both of the locations show the shift in TS space, but the shift did not reach deep waters until year 15 at the central subpolar gyre. From the observational point of view, there indeed was a shift in TS space in deep waters in the northern North Atlantic between 1972 and 1981 as reported by Swift (1984). This freshening is suggested by this study to be directly linked to the GSA and to a subsequent slowdown of meridional overturning as also discussed below.

#### e. Anomalies in freshwater content

As already referred in section 3c, the GSA event can influence the MOC all the way to the southern boundary and part of these changes persist for the remainder of the experiment, such as the decrease in MOC. The GSA-related changes happen within 5–6 yr, thus the influence

of the southern boundary will be felt in the limited-area model results rather quickly. One should be cautious about interpreting the model results beyond year 6, but at the same time the GSA2 experiment demonstrates that the GSA may have had a significant effect on the deep circulation beyond the North Atlantic Ocean.

Dickson et al. (1988) estimated that the GSA had a freshwater anomaly of about  $2300 \text{ km}^3$  when it passed through the Labrador Sea. As shown in section 3a the simulated freshwater from excess ice export through the Denmark Strait is about half of that. In the model there is some export of the meltwater from the GIN Seas to contribute to the difference. The freshwater accumulation between the boundaries marked in Fig. 1 in GSA1 and GSA2 runs referenced to their undisturbed parallel runs is shown Fig. 12a. Within 2 yr both runs have accumulated  $2000 \text{ km}^3$ , any further accumulation is difficult to explain by freshwater transport from GIN Seas because the GIN Seas return to near-normal conditions within 2–3 yr (Fig. 10b). Thus the increase is due to the accumulation of local precipitation because of weak-

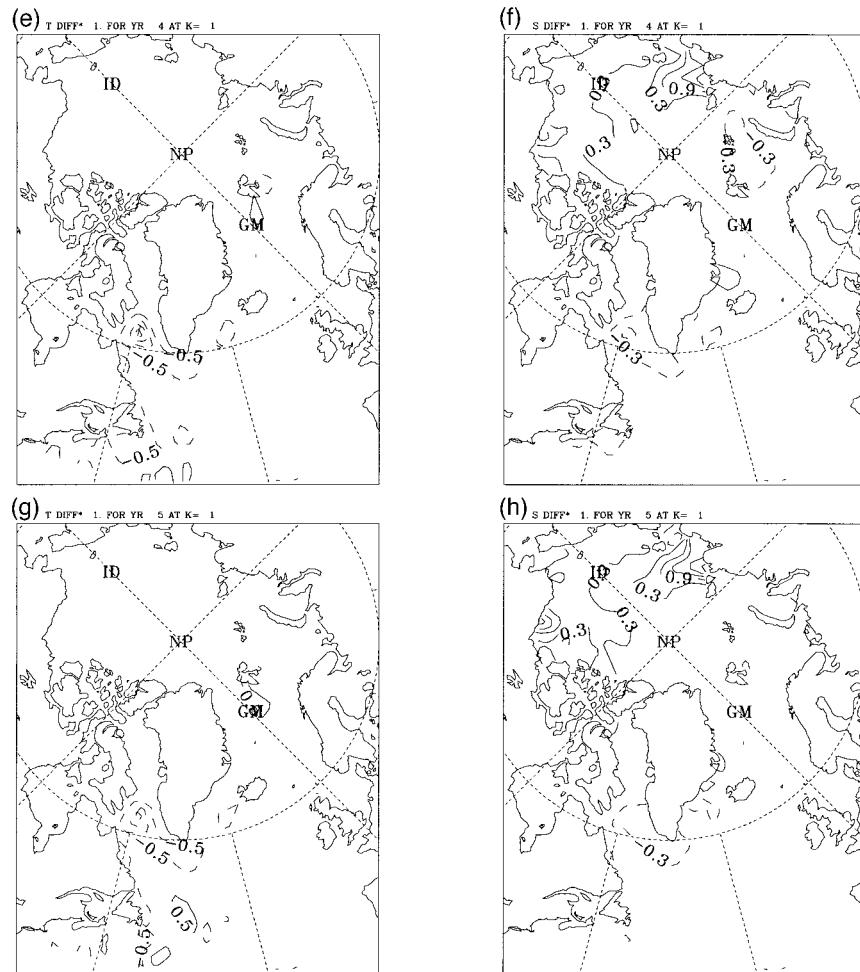


FIG. 9. (Continued)

er convection, which would mix the freshwater into the deep ocean and into DWBC. For instance, the freshwater content in GSA1 does not reach maximum until year 6 when reversal to convective conditions is already under way. In the GSA2 run the freshwater accumulation is more rapid although forcing is the same as in GSA1. One reason is that in GSA1, the basic state already has an MOC that gets weaker with time because the buoyancy flux in the subpolar gyre cannot maintain a strong production of LSW. A part of the difference could be explained by the circulation changes associated with GSA2 where the North Atlantic Current weakens and does not provide as much saline waters to the subpolar gyre. After year 6 there is a transition to ever-freshening conditions in GSA2, which is associated with the changed MOC extending to the southern boundary. The drift is nearly linear in time although there is a weak freshening event at year 12, which represents the recirculating remains of the GSA.

The change of the net freshwater content anomaly in the whole model due to the variations in MOC is shown in Fig. 12b. The influence of the high-latitude processes

is felt nearly immediately at the southern boundary due to the propagation of topographic Rossby waves modifying the stratification and the geostrophic velocities. The changes are rather small for the first 2 yr but gain amplitude rapidly once the advective changes in the DWBC arrive (at  $10 \text{ cm s}^{-1}$  it takes 2 yr to go from  $45^\circ\text{N}$  to  $15^\circ\text{S}$ ). While the GSA1 run returns slowly toward its reference run values, the GSA2 has a linear trend because of the persistent decrease of  $0.5\text{--}1.0 \text{ Sv}$  in MOC extending from the midlatitudes to the southern boundary. The less intense MOC has two consequences in GSA2 leading to accumulation of freshwater in the system: 1) the slower southward movement of the fresh DWBC waters, which are now fresher than in the control run and 2) at the same time the northward flux (across the equator) of salt is weakened because of the weaker overturning. The freshwater accumulation in the model basin, in the GSA2, is distributed so that it mainly occurs in the subpolar and polar areas while the Tropics–subtropics are becoming more saline. The freshwater anomaly in the areas from the equator to about  $45^\circ\text{N}$  (the southern boundary of the subpolar gyre; Fig. 12c) and

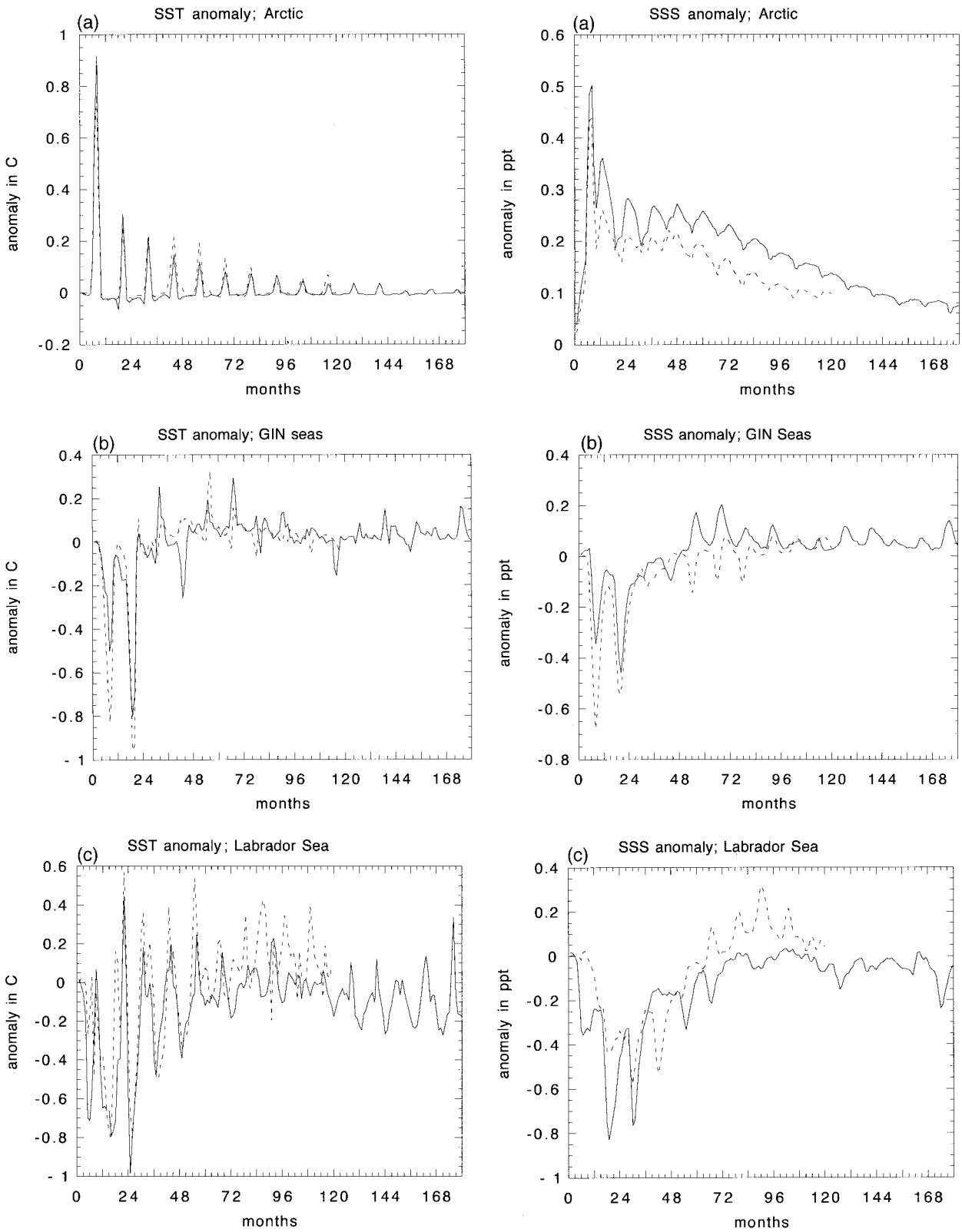


FIG. 10. Area-averaged SST and SSS anomalies [computed as (GSA–control experiment) for (a) Arctic, (b) GIN Seas, and (c) Labrador Sea (west of 30°W with northern and southern boundaries defined in Fig. 1). Dashed line refers to GSA1 and solid line to GSA2.

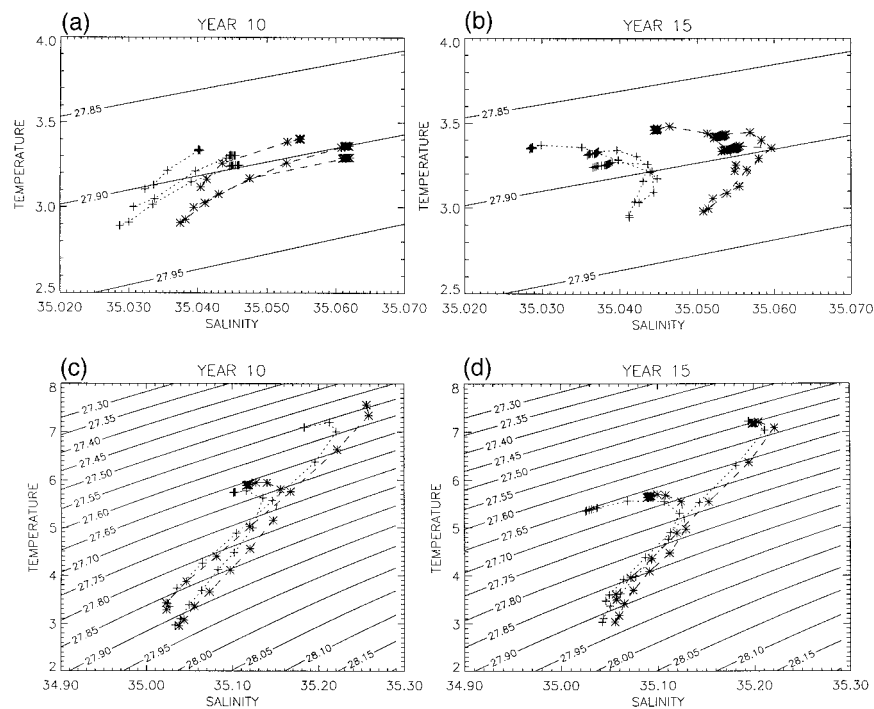


FIG. 11. TS diagrams in experiment 2 (dashed) and GSA2 (dotted) (a) for three points east off Newfoundland at year 10 and 15, (b) for two central subpolar gyre locations at year 10 and 15. Density field is contoured with  $0.05 \sigma_0$ -units.

north of the Nordic Sills (Fig. 12d; north of the northern boundary of the subpolar gyre) show the nonuniform nature of the drift. In fact, this distribution of freshwater is supported by the analysis by Lazier (1988), which suggests that the freshwater anomaly associated with the GSA did not disperse much outside subpolar and polar areas. In Fig. 12d the GSA2 polar anomaly shows the maximum salinization to correspond to about  $1500 \text{ km}^3$  freshwater deficit at the same time when the subpolar gyre freshwater excess has reached  $3000 \text{ km}^3$ . This also supports the conclusion that local precipitation is accumulating due to weak convection in the subpolar gyre.

#### 4. Conclusions

The model simulation of an idealized GSA event presented here shows how one single freshwater disturbance as a result of excess sea ice export from the Arctic can have far-reaching consequences in the North Atlantic thermohaline system and in the meridional heat transport. The important factors in the ocean response are the amplitude, duration, and timing of the sea ice pulse: about  $1000 \text{ km}^3$  of sea ice exits through the Denmark Strait within 6 months during fall and early winter. If this amount would have been distributed evenly throughout 1 yr, a very weak response would have resulted: less than  $0.5 \text{ Sv}$  change in overturning cell as discussed by Power et al. (1994). The study is not pre-

senting the GSA as a part of an interdecadal cycle, but as a process involving sea ice that can influence decadal to interdecadal variability in the subtropical and subpolar North Atlantic. The key to the variability is convection, or lack of it, in the Labrador Sea and its freshwater reservoir.

In normal conditions, convection in the subpolar gyre would mix fresh surface waters down to be advected back to the lower latitudes through overturning circulation. An excess freshwater input from sea ice melt can disrupt this deep mixing process, which leads to further freshening. Thus, the initial anomaly amplifies itself because the local precipitation, the net  $P - E$  is positive in the subpolar gyre, is accumulating at the surface. The extent and influence of the anomaly spreads beyond the deep convective area near Newfoundland and the salinity anomaly gets enhanced further, because all parts of the subpolar gyre contribute to the modification process. This domino effect in the context of thermal forcing has been discussed by Lenderink and Haarsma (1994) and shown by Rahmstorf (1995a,b) to apply to changes in hydrological forcing also. The recovery from such an event will take several years or decades depending on the oceanic state before advection and diffusion remove the salinity anomaly. Meanwhile the influence of the GSA propagates to the subtropics via the boundary currents and baroclinic adjustment to the new boundary currents. The resulting new quasi-equilibrium may not be the same as that of the undisturbed control run, which

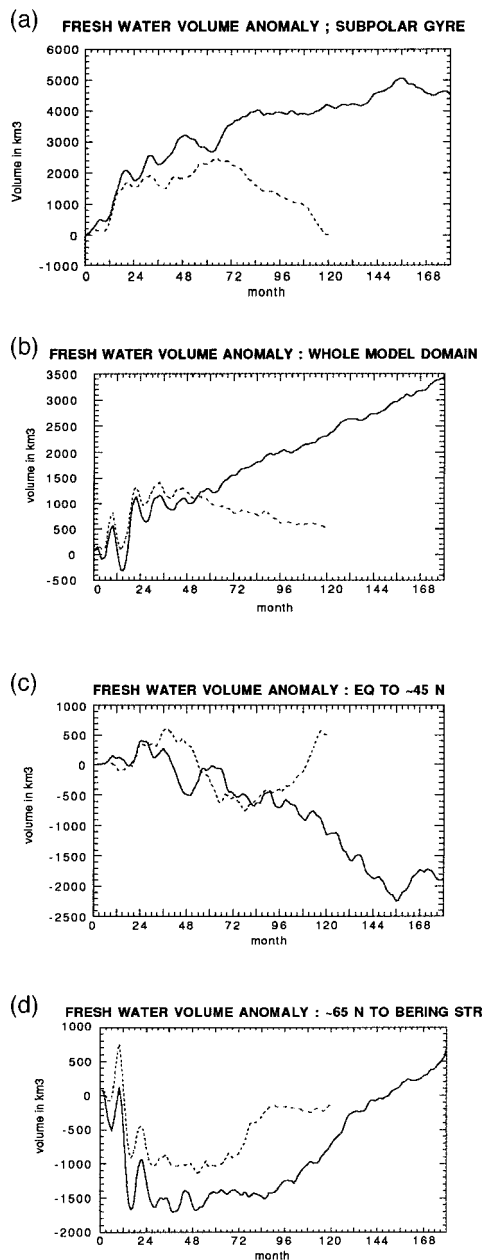


FIG. 12. Freshwater volume anomalies for (a) subpolar gyre, (b) total model area, (c) from the equator to southern boundary of subpolar gyre (see Fig. 1), and (d) north of the northern boundary of the subpolar gyre. Dashed line refers to GSA1 and solid line to GSA2.

is the case in the experiment experiment 2–GSA2 as there exists a hysteresis of thermohaline circulation states that depend only on the initial state (Rahmstorf 1995b).

The maximum meridional heat transport changes associated with the simulated GSA event, 0.2 PW, are order of 20% of climatological values in subtropics and even higher in the subpolar area. Ezer et al. (1995) fail to show such a difference between the 1950s and 1970s,

but it is doubtful that their quasi-diagnostic calculation and use of 5-yr averaged data could show an event peaking within 5 yr. This model shows weakening of the Gulf Stream system as suggested by diagnostic studies, but lacking a southern recirculation gyre, the model response is not so well defined as in Greatbatch et al. (1991). Simulations do show that the changes in the vertically integrated transport are limited to the Gulf Stream–North Atlantic Current system.

The strong oceanic response can be achieved via a temporary redistribution of the surface freshwater flux at high latitudes through ice transport where the decreased ice cover in the Arctic will lead to increased ice production and a more saline mixed layer while the subpolar gyre gets fresher from melting ice. Thus a negative feedback toward normal conditions in the subpolar gyre exists within the polar–subpolar system as the salinized Arctic mixed layers eventually arrive to restart convection in the Labrador Sea. While the system appears to return to normal operation after a few years, the event has left a TS signal in the deep waters and in the MOC. The shift in TS space is supported by observations (Swift 1984) that show a freshening and cooling of deep waters between 1972 and 1981.

The two experiments presented here, GSA1 and GSA2, differ significantly in their responses to the same sea ice disturbance. The fundamental difference is that the basic state in the experiment 1–GSA1 experiment has a severely compromised LSW formation in comparison to experiment 2–GSA2. Thus, in experiment 1–GSA1 any further addition of freshwater to the subpolar gyre has an ever-diminishing effect on the production and maintenance of the LSW and deeper water masses. This behavior of the two runs has more general importance for numerical simulation of thermohaline effects in the North Atlantic system: It is essential that in a climatological state an ocean model produces LSW and maintains a stable amount of LSW and deeper waters, otherwise a significant part of the oceanic response to atmospheric and sea ice forcing variability can be poorly simulated.

*Acknowledgments.* I would like to thank Dr. Jiayan Yang for the critical reading of this manuscript. I appreciate very much the helpful comments by Dr. Peter Rhines and the anonymous reviewer. Also thanks are due to Lena Marshak for programming and computer support. This work was supported by NASA Headquarters and the NOAA ACCP program.

#### REFERENCES

- Aagaard, K., and E. C. Carmack, 1989: The role of sea ice and other fresh water in the Arctic circulation. *J. Geophys. Res.*, **94**, 14 485–14 498.
- Blumberg, A. F., and G. L. Mellor, 1987: A description of a three-dimensional coastal ocean circulation model. *Three Dimensional Coastal Ocean Models*, N.S. Heaps, Ed., Amer. Geophys. Union, 1–16.

- Dickson, R. R., J. Meincke, S.-A. Malmberg, and A. J. Lee, 1988: The "Great Salinity Anomaly" in the northern North Atlantic 1968–1982. *Progress in Oceanography*, Vol. 20, Pergamon Press, 103–151.
- , J. Lazier, J. Meincke, P. Rhines, and J. Swift, 1996: Long-term coordinated changes in the convective activity of the North Atlantic. *Progress in Oceanography*, Vol. 38, Pergamon Press, 241–295.
- Ezer, T., G. L. Mellor, and R. J. Greatbatch, 1995: On the interpentadal variability of the North Atlantic Ocean: Model simulated changes in transport, meridional heat flux and coastal sea level between 1955–1959 and 1970–1974. *J. Geophys. Res.*, **100**, 10 559–10 566.
- Greatbatch, R. J., and J. Xu, 1993: On the transport of volume and heat through sections across the North Atlantic: Climatology and the pentads 1955–1959, 1970–1974. *J. Geophys. Res.*, **98**, 10 125–10 143.
- , A. F. Fanning, A. D. Goulding, and S. Levitus, 1991: A diagnosis of interpentadal circulation changes in the North Atlantic. *J. Geophys. Res.*, **96**, 22 009–22 023.
- Häkkinen, S., 1993: An Arctic source for the Great Salinity Anomaly: Simulation of the Arctic ice ocean system for 1955–1975. *J. Geophys. Res.*, **98**, 16 397–16 410.
- , 1995: Simulated interannual variability of the Greenland Sea deep water mass formation and its connection to surface forcing. *J. Geophys. Res.*, **100**, 4761–4770.
- , and G. L. Mellor, 1992: Modeling the seasonal variability of the coupled Arctic ice-ocean system. *J. Geophys. Res.*, **97**, 20 285–20 304.
- Hallberg, R., and P. Rhines, 1996: Buoyancy driven circulation in an ocean basin with isopycnals intersecting the sloping boundary. *J. Phys. Oceanogr.*, **26**, 913–940.
- Hurrell, J. W., 1995: Decadal trends in the North Atlantic Oscillation: Regional temperatures and precipitation. *Science*, **269**, 676–679.
- Kawase, M., 1987: Establishment of deep circulation driven by deep water production. *J. Phys. Oceanogr.*, **17**, 2294–2316.
- Lazier, J. R. N., 1980: Oceanographic conditions at Weather Station Bravo, 1960–1974. *Atmos.–Ocean*, **18**, 18 227–18 238.
- , 1988: Temperature and salinity changes in the deep Labrador Sea, 1962–1986. *Deep-Sea Res.*, **35**, 1247–1253.
- Lenderink, G., and R. J. Haarsma, 1994: Variability and multiple equilibria of the thermohaline circulation associated with deep-water formation. *J. Phys. Oceanogr.*, **24**, 1480–1493.
- Levitus, S., 1982: *Climatological Atlas of the World Ocean*. NOAA Professional Paper 13, 173 pp.
- , 1989: Interpentadal variability of temperature and salinity at intermediate depth of the North Atlantic Ocean, 1970–1974 versus 1955–1959. *J. Geophys. Res.*, **94**, 6091–6131.
- Manabe, S., and R. J. Stouffer, 1995: Simulation of abrupt climate change induced by freshwater input to the North Atlantic Ocean. *Nature*, **378**, 165–167.
- Mauritzen, C., and S. Häkkinen, 1997: Influence of the sea ice on the thermohaline circulation in the Arctic–North Atlantic Ocean. *Geophys. Res. Lett.*, **24**, 3257–3260.
- , and —, 1998: On the relationship between dense water formation and the "meridional overturning cell." *Deep-Sea Res.*, in press.
- Mellor, G. L., and T. Yamada, 1982: Development of a turbulence closure model for geophysical fluid problems. *Rev. Geophys.*, **20**, 851–875.
- , and L. H. Kantha, 1989: An ice-ocean coupled model. *J. Geophys. Res.*, **94**, 10 937–10 954.
- Pocklington, R., 1987: Arctic rivers and their discharges. *SCOPE/UNEP Sonderb.*, **64**, 261–268.
- Power, S. B., A. M. Moore, D. A. Post, N. R. Smith, and R. Kleeman, 1994: Stability of North Atlantic Deep Water formation in a global ocean general circulation model. *J. Phys. Oceanogr.*, **24**, 904–916.
- Rahmstorf, S., 1995a: Multiple convection patterns and thermohaline flow in an idealized OGCM. *J. Climate*, **8**, 3028–3039.
- , 1995b: Bifurcations of the Atlantic thermohaline circulation in response to changes in the hydrological cycle. *Nature*, **368**, 145–149.
- Rasmusson, E. M., and K. Mo, 1996: Large scale atmospheric moisture cycling as evaluated from NMC global analysis and forecast products. *J. Climate*, **9**, 3276–3297.
- Russell, G. L., and J. R. Miller, 1990: Global river runoff calculated from a global atmospheric general circulation model. *J. Hydrol.*, **117**, 241–254.
- Swift, J. H., 1984: A recent TS shift in the deep water of the northern North Atlantic. *Climate Processes and Climate Sensitivity, Geophys. Monogr.*, No. 29, Amer. Geophys. Union, 39–47.
- Trenberth, K., J. G. Olson, and W. G. Large, 1989: A global ocean wind stress climatology based on ECMWF analyses. NCAR Tech. Note NCAR/TN-338+STR, 93 pp.